Current Biology 20, 1145–1153, July 13, 2010 ©2010 Elsevier Ltd All rights reserved DOI 10.1016/j.cub.2010.05.049

Article

Transient Frictional Slip between Integrin and the ECM in Focal Adhesions under Myosin II Tension

Yvonne Aratyn-Schaus[1] and Margaret L. Gardel[1,2,3,*]
[1]Institute for Biophysical Dynamics
[2]James Franck Institute
[3]Department of Physics
University of Chicago, Chicago, IL 60637

Summary

Background: The spatiotemporal regulation of adhesion to the extracellular matrix is important in metazoan cell migration and mechanosensation. Although adhesion assembly depends on intracellular and extracellular tension, the biophysical regulation of force transmission between the actin cytoskeleton and extracellular matrix during this process remains largely unknown.
Results: To elucidate the nature of force transmission as myosin II tension is applied to focal adhesions, we correlated the dynamics of focal adhesion proteins and the actin cytoskeleton to local traction stresses. Under low extracellular tension, newly formed adhesions near the cell periphery underwent a transient retrograde displacement preceding elongation. We found that myosin II-generated tension drives this mobility, and we determine the interface of differential motion, or "slip," to be between integrin and the ECM. The magnitude and duration of both adhesion slip and associated F-actin dynamics is strongly modulated by ECM compliance. Traction forces are generated throughout the slip period, and adhesion immobilization occurs at a constant tension.
Conclusions: We have identified a tension-dependent, extracellular "clutch" between integrins and the extracellular matrix; this clutch stabilizes adhesions under myosin II driven tension. The current work elucidates a mechanism by which force transmission is modulated during focal adhesion maturation.

Introduction

Focal adhesions (FAs) form hierarchical connections between the F-actin cytoskeleton and the extracellular matrix (ECM) to transmit mechanical forces across the plasma membrane. Force generated within the F-actin cytoskeleton and transmitted at FAs exert traction on the ECM and are important in cell migration and ECM remodeling [1, 2]. In turn, the mechanical properties of the ECM are sensed by adherent cells and directly affect the morphology of FAs and the F-actin cytoskeleton [3]. Cellular force sensing is thought to be dominated through the regulation of FA assembly and growth by both intracellular and extracellular forces [4–7]. Thus, an intricate feedback exists between the F-actin cytoskeleton, ECM mechanics, traction force generation, and FA assembly.

FA assembly is thought to modulate force transmission by regulating the coupling of F-actin motion to the underlying ECM. Near the cell periphery, F-actin polymerization drives a rapid retrograde flow of a branched, dendritic network, termed the lamellipodium. Proximal to the lamellipodium, the F-actin cytoskeleton transitions into a contractile organelle, termed the lamella, where retrograde flow is mediated by myosin II. In the absence of FA formation, lamellar retrograde flow is quite rapid and uniform throughout the cell body [8, 9]. During FA assembly, F-actin retrograde flow slows [8], and traction stress builds on the ECM [10]. This process is consistent with the idea that FAs serve as a molecular "clutch" between dynamic F-actin and the immobile ECM [11–13].

Identification of molecular interactions that regulate the molecular clutch during FA assembly is critical to further understanding of cellular force transduction. Generally, clutch regulation could occur intracellularly, via modulation of FA proteins that link F-actin to integrins, and/or extracellularly, via modulation of integrin-ECM binding. During FA initiation, talin plays an important role in regulating this intracellular linkage, and talin-deficient cell lines have impaired integrin-ligand binding, enhanced retrograde F-actin flow, and reduced traction stress [9, 14]. Likewise, in elongated FAs, points of disconnect between F-actin and integrins are α-actinin and vinculin [15, 16]. The extent to which these proteins modulate intracellular clutch engagement as tension is built during FA assembly and growth is unknown. Furthermore, although extracellular clutch regulation between the integrin and the ECM has been suggested [12], no direct observations have been made. Thus, the components of the molecular clutch during tension-dependent adhesion assembly remain unknown.

In this study, we identify a tension-dependent clutch at the integrin-ECM interface on physiologically flexible substrates. At low levels of tension, FAs undergo rapid, micron-scale retrograde displacement relative to the ECM while transmitting traction force; like others, we term this behavior "frictional slip" [11]. When the ECM stiffness decreases, the magnitude and duration of frictional slip is enhanced but adhesions immobilize at similar levels of tension. Once this extracellular clutch is engaged, F-actin moves relative to FA components. Thus, actomyosin retrograde flow and ECM mechanics are coordinated to regulate an extracellular clutch during the initial stages of tension-dependent stabilization of FAs.

Results

ECM Compliance Regulates the Mobility of Nascent FAs

To confirm that the morphological changes associated with FA assembly in human osteosarcoma (U2OS) cells are similar to those observed in other cell types, we used time-lapse microscopy to image the assembly of GFP-paxillin-rich adhesions near the periphery of cells plated on fibronectin-coated glass coverslips. We observed the appearance of newly formed, or nascent, adhesions near the leading cell edge as small ($\sim$0.5 μm diameter) fluorescent spots (Figure 1, upper panel). These nascent adhesions appeared to be stationary with respect to the underlying coverslip and, over the course of 15–20 min, elongated rearward into larger plaques with a length of 3–5 μm. These morphological events are in accordance with published studies of FA maturation on rigid, glass substrates in numerous cell types [2, 17, 18].

*Correspondence: gardel@uchicago.edu

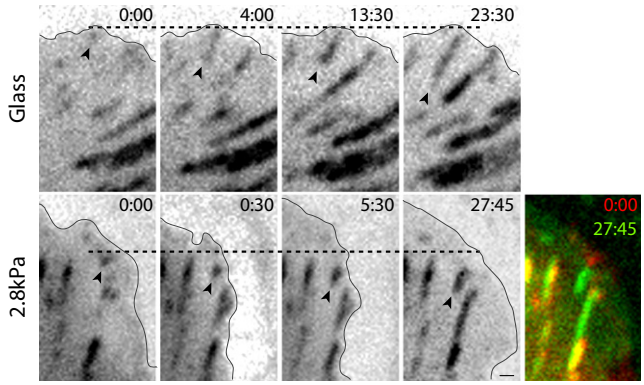

Figure 1. FA Maturation on Rigid and Compliant Substrata

(Upper panel) On glass, a GFP-paxillin punctum appears near the cell edge, remains immobilized, and elongates within minutes. (Lower panel) On a compliant substrate (2.8 kPa gel), a GFP-paxillin punctum appears near the cell edge and undergoes retrograde displacement prior to immobilization and elongation. Dashed lines highlight initial location of the distal edge of FA puncta. Arrowheads indicate proximal end of FA. A solid black line indicates the cell boundary. Color-combined image of FA at 0:00 (red) and 27:45 (green). Time stamp is in min:s. The scale bar represents 1 μm.

To explore how ECM stiffness impacts FA assembly, we visualized FA dynamics in U2OS cells plated on fibronectin-coated polyacrylamide gels with a shear elastic modulus of 2.8 kPa, which resembles the stiffness of physiological tissue [3]. On compliant gels, cells spread and formed elongated FA plaques similar in size to those found in cells plated on fibronectin-coated glass coverslips; FA maturation consisted of the appearance of small (~0.5 μm) fluorescent spots near the cell periphery and subsequent elongation over a period of 15–20 min. However, on compliant gels, nascent adhesions underwent a rapid, retrograde displacement from their origin of appearance prior to immobilization to the ECM (Figure 1, lower panel). This retrograde movement was only seen in nascent adhesions within 30–90 s after appearance, and it occurred in a majority of the nascent adhesions observed (65%, n_{FA} = 39, n_{cell} = 6). The magnitude of retrograde displacement was 0.67 ± 0.33 μm (n_{FA} = 39, n_{cell} = 6) and, once immobilized, a majority (77%, n_{FA} = 39, n_{cell} = 6) of adhesions elongated proximally. Thus, on compliant matrices, a rapid, transient rearward translocation of newly formed adhesion puncta usually precedes growth to an elongated FA plaque.

Blebbistatin Treatment and Removal as a Methodology for Studying Myosin II-Driven FA Maturation

The retrograde movement of nascent adhesions observed on compliant matrices suggests a probable role for myosin II contractility. To investigate this, we designed an experimental approach to isolate and synchronize myosin II-driven adhesion maturation by perfusion and removal of the myosin II ATPase inhibitor blebbistatin [19]. In combination with traction force and high-resolution confocal microscopy of GFP-actin and mApple-paxillin (Experimental Procedures), this enabled a characterization of both cytoskeletal dynamics and force transmission at adhesions during the first steps of myosin II-impinged tension.

Under control conditions, condensed actin bundles ranging from 5 to 70 μm in length terminated in elongated adhesions with an average length of 3 μm (Figure 2; Figures S1 and S3C); the average traction stress exerted at peripheral FAs was 150 Pa (Figure 2; Figure S3B). After treatment with 25–50 μM of blebbistatin for 30 min, only small paxillin- and vinculin-rich puncta that resembled nascent adhesions remained (Figure 2; Figures S1–S3). Under blebbistatin treatment, actomyosin bundles disassembled, and dense "patches" of actin colocalized with adhesions at the lamellipodial-lamellar border (LLB; Figure 2; Figures S1–S3). Immunostained samples revealed an F-actin meshwork with a dense ribbon of F-actin at the LLB and myosin II puncta, presumably minifilaments [20], across the lamellar region (Figure S1). Traction stresses were constrained to the lamellipodial base and were reduced to 20–30 Pa (Figure 2; Figure S3).

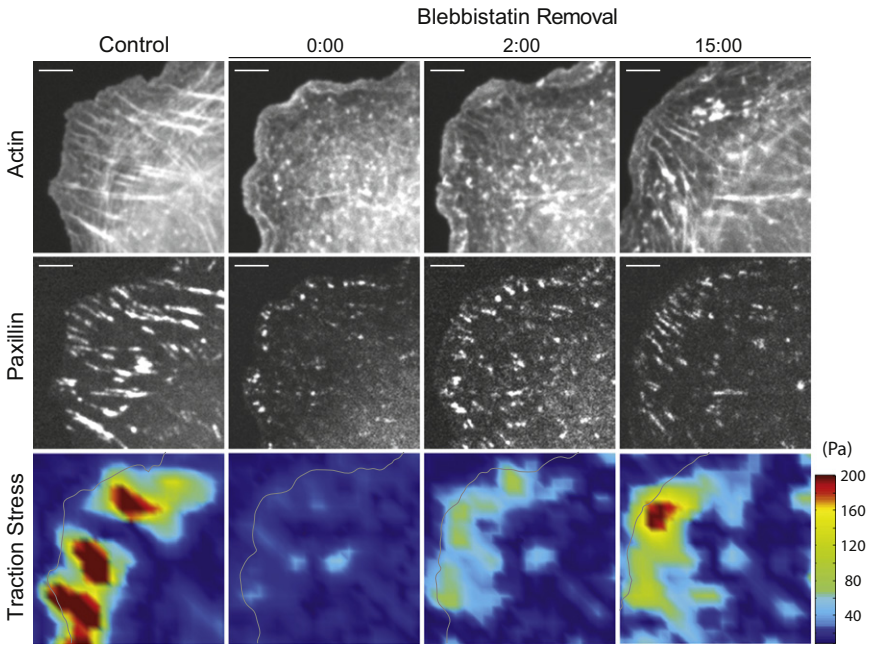

Figure 2. Cytoskeletal Remodeling and Traction-Stress Recovery upon Myosin Reactivation by Blebbistatin Removal

Images of GFP-actin (top), mApple-paxillin (middle), and traction-stress magnitude at times prior to blebbistatin treatment (control) and at times indicated after blebbistatin removal. Time is indicated in min:s. A gray line indicates the cell boundary. The scale bar represents 5 μm.

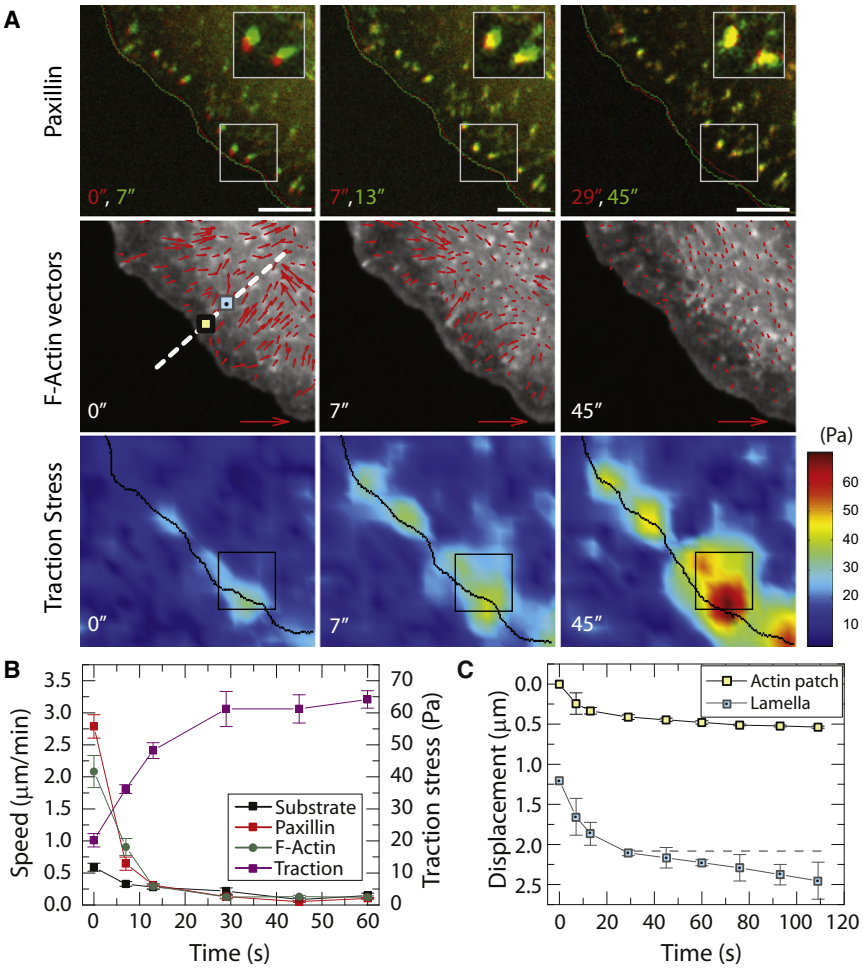

Figure 3. F-Actin and FAs Move Retrogradely as Myosin II Is Reactivated

(A) (Top) Color-combined images of mApple-paxillin at successive times after blebbistatin removal, early (red) and late (green) times. Insets show magnification of outlined regions. The scale bar represents 5 μm. (Middle) GFP-actin images overlaid with actin flow vectors (red arrows). Time indicates the initial time point used in the velocity calculation. A red arrow indicates trajectory scale = 4.5 μm/min. A dashed white line indicates a typical linescan across cell front used in analysis; the location of adhesion and actin patches (yellow square with black outline) and lamellar actin (light blue square) is shown. (Bottom) Heat-scale map of traction stress with the scale bar indicated at right (from blue to red). Times are indicated in seconds.

(B) Traction stress (violet squares), F-actin flow (green circles), paxillin speed (red), and substrate speed (black squares) over time after blebbistatin removal. F-actin flow was tracked at actin patches associated with FA. Data reflect mean plus standard error for n_{FA} = 26 and n_{cell} = 5.

(C) Displacement of actin patches colocalized with adhesions (yellow square, black outline) and at 1.2 μm proximal to adhesion puncta within the lamella (blue square). Approximate locations of these data points are indicated in (A), middle panel. The horizontal dashed line is a line of zero slope. Data plotted in figures reflect the mean plus standard error about the mean.

We synchronized myosin II-driven adhesion maturation across the entire cell by deactivating blebbistatin by means of drug removal and imaging with 488 nm light [21] (Movie S1 and Movie S2). Within 15 s, the traction stress at paxillin-rich adhesions increased to 57 ± 13 Pa, and a marginal increase in the average adhesion length was resolved (Figure S3). Two minutes after blebbistatin removal, the traction stress exerted at individual adhesions had increased by approximately 4-fold, adhesions had elongated by roughly twice their myosin II-independent length, and short actin bundles were resolved (Figure 2; Figure S3). Fifteen minutes after blebbistatin removal, adhesions had elongated to 80% of their control length, condensed myosin-rich actin bundles were observed to span the cell body, and traction stresses had recovered to the same order of magnitude as pre-blebbistatin levels (Figures 2; Figures S1 and S3). Thus, blebbistatin treatment and removal has a reversible effect on cytoskeletal organization and can be used for studying the process of myosin II-driven maturation of FAs [6, 22].

F-Actin and FA Dynamics Reveal Frictional Slip at the FA-ECM Interface

To examine the mobility of adhesions upon blebbistatin removal, we compared pairs of mApple-paxillin images in an aligned time-lapse sequence (Figure 3A; Movie S3). Similar to newly formed adhesions in drug-free conditions, adhesion puncta moved retrogradely upon removal of blebbistatin. Comparing images obtained immediately (0 s) and 7 s after blebbistatin removal indicated that the mApple-paxillin puncta were displaced toward the cell center, whereas the location of the cell edge had not changed significantly (indicated by line traces in Figure 3A). Between 7 and 13 s after removal, retrograde movement of adhesions was substantially reduced. At later times, the distal tip of adhesions did not translocate (Figure 3A).

To quantify this motion, we identified the centroids of the mApple-paxillin puncta and calculated rates of displacement. Line scans across individual adhesions during frictional slip revealed a Gaussian intensity profile with a full-width half maximum of ~300 nm and a significant signal-to-noise ratio (Figure S4), indicating that these features were nearly diffraction limited and amenable to computational tracking algorithms that track the centroid with sub-pixel resolution and provide a resolution of mobility on the order of 0.02 μm/min [23, 24]. Initially, between 0 and 7 s, the adhesion moved retrogradely with a speed of 2.7 μm/min (Figure 3B). Within 15 s of blebbistatin removal, the apparent movement of paxillin-rich puncta subsided to values near our resolution limit. Because cells were adhered to compliant substrates, it is possible that some retrograde movement could be accommodated by substrate deformation. However, fiducial markers in the top surface of the substrate underlying adhesion puncta moved less than 1 μm/min, and there was a rapid decay thereafter (Figure 3B); movement of fibronectin that was adhered to the top surface of the substrate moved at rates similar to that of the substrate (Figure S4). Thus, by 15 s after blebbistatin removal, the apparent retrograde motion of the paxillin is abrogated with respect to the underlying fibronectin-coated substrate and defines FA immobilization.

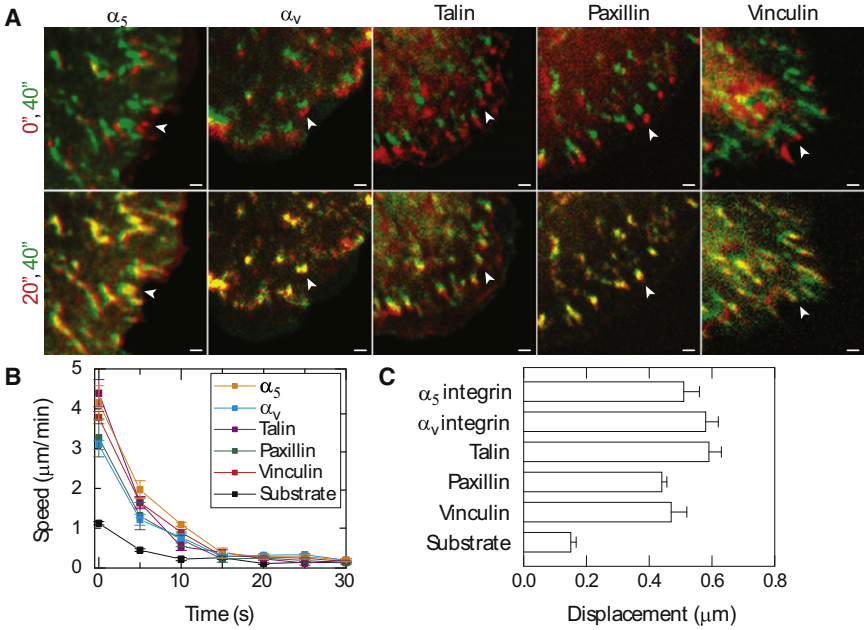

Figure 4. FA Displacement Occurs at the Integrin-ECM Interface

(A) Color-combined images of FA proteins upon blebbistatin inactivation: (top) 0 s (red) and 40 s (green) and (bottom) 20 s (red) and 40 s (green). The scale bar represents 1 μm. Arrowheads indicate adhesion puncta.

(B) Speeds of FA proteins and beads in substrate over time after blebbistatin inactivation.

(C) Total displacement of adhesion proteins and substrate prior to adhesion immobilization. There is no statistically significant difference between FA proteins; substrate displacement is statistically significantly different from FAs ($p < 0.0001$). Data reflect the mean and standard error for all samples. Sample sizes are as follows: α_5 ($n_{FA} = 8$; $n_{cell} = 6$), α_v ($n_{FA} = 9$; $n_{cell} = 4$), talin ($n_{FA} = 6$; $n_{cell} = 3$), paxillin ($n_{FA} = 26$; $n_{cell} = 16$), and vinculin ($n_{FA} = 12$; $n_{cell} = 3$).

Data plotted in the figure reflect the mean plus standard error about the mean.

To observe F-actin dynamics during blebbistatin removal, we monitored fiducial marks of GFP-actin over time. Immediately after blebbistatin removal, actin patches colocalized with adhesion puncta at the LLB (yellow square, Figure 3A) and underwent a rapid, coherent retrograde movement, decreasing from 2.1 μm/min to < 0.1 μm/min within 15 s of blebbistatin removal (Figures 3A and 3B; Figure S5A). Thus, actin patches stabilized ~0.5 μm proximal from their starting location (Figure 3C). Lamellar actin, located approximately 1.2 μm proximal to these patches (blue square, Figure 3A), exhibited similar, but slightly enhanced, retrograde flow dynamics and stabilized at roughly 30 s to a steady-state retrograde flow of 0.25 μm/min, the value observed in compact stress fibers [25] (Figure S5A). Within 15 s after blebbistatin removal, lamellar F-actin moved retrogradely ~1 μm and continued to move toward the cell center at later times (Figure 3C). Thus, the distance between the actin patches that colocalized with adhesions and fiduciary marks in lamellar actin increased under myosin-driven dynamics.

The traction stress exerted on the extracellular matrix increased monotonically from about 20 Pa to 50 Pa as mApple-paxillin underwent retrograde movement (Figures 3A and 3B). Interestingly, during this time, we observed an inverse relationship between the traction stress and F-actin retrograde flow rate, such that traction stress increased while F-actin retrograde flow speed decayed (Figure S5B); this relationship is consistent with known mechanochemistry of individual myosin II motors (Supplemental text; Figure S5). Thus, even while FAs move relative to the underlying matrix, mechanical forces are transmitted to the extracellular matrix. We refer to this transient state as myosin II-driven "frictional slip" of adhesion puncta, a phenomenon previously observed in filopodial adhesions [11].

Frictional Slip in Nascent Adhesions Occurs between Integrin and the ECM

Because FAs are multicomponent ensembles that contain a diverse group of actin and ECM binding proteins [26, 27], we sought to determine whether varying retrograde flow dynamics occur at different components during frictional slip. We investigated two classes of integrins, α_v and α_5, known to bind fibronectin, as well as two FA proteins, talin [9, 14] and vinculin [15, 16, 28], which establish a molecular link between integrin and actin. We found that all of these proteins underwent retrograde motion comparable to that of paxillin within the first 20 s after blebbistatin removal and were immobilized thereafter (Figure 4A, Movie S4 and Movie S5). The retrograde dynamics of different FA proteins were highly correlated, as measured by Pearson's correlation coefficient (0.98), and all proteins became immobilized to the substrate after approximately 15 s (Figure 4B). Furthermore, the total displacement of each protein population prior to substrate engagement was similar; the average displacement was 0.5 μm, approximately 4-fold greater than that of the underlying substrate (Figure 4C). These data indicate that a diverse set of FA-associated proteins, ranging from associated actin to integrin, displace as a collective unit prior to their immobilization and that a predominant slip occurs at the interface between integrin and the ECM.

FRAP Reveals Stable Association of α_v Integrin to Adhesion Puncta during Slip

Micron-sized movements of integrin relative to the underlying substratum occur simultaneously with increases in traction. Because these movements are too large to be accommodated by individual bond deformation or stretching, we hypothesize this motion could result from either polarized remodeling [29] or the nature of binding kinetics between the integrin and ECM [11, 30]. For polarized remodeling, dissociation of integrin from the distal tip is balanced by incorporation of new integrin at the proximal end to result in apparent motion [31]. In this scenario, we would expect nearly complete exchange of integrins with the diffuse population during frictional slip, as has been observed in polarized remodeling of mature FAs over long time scales [29]. By contrast, if the integrins are stably bound to intracellular FA components, integrin exchange might not occur.

We utilized fluorescence recovery after photobleaching (FRAP) to determine whether integrins are stably associated within the adhesion puncta during frictional slip. We bleached GFP-α_5 and GFP-α_v upon blebbistatin removal and measured

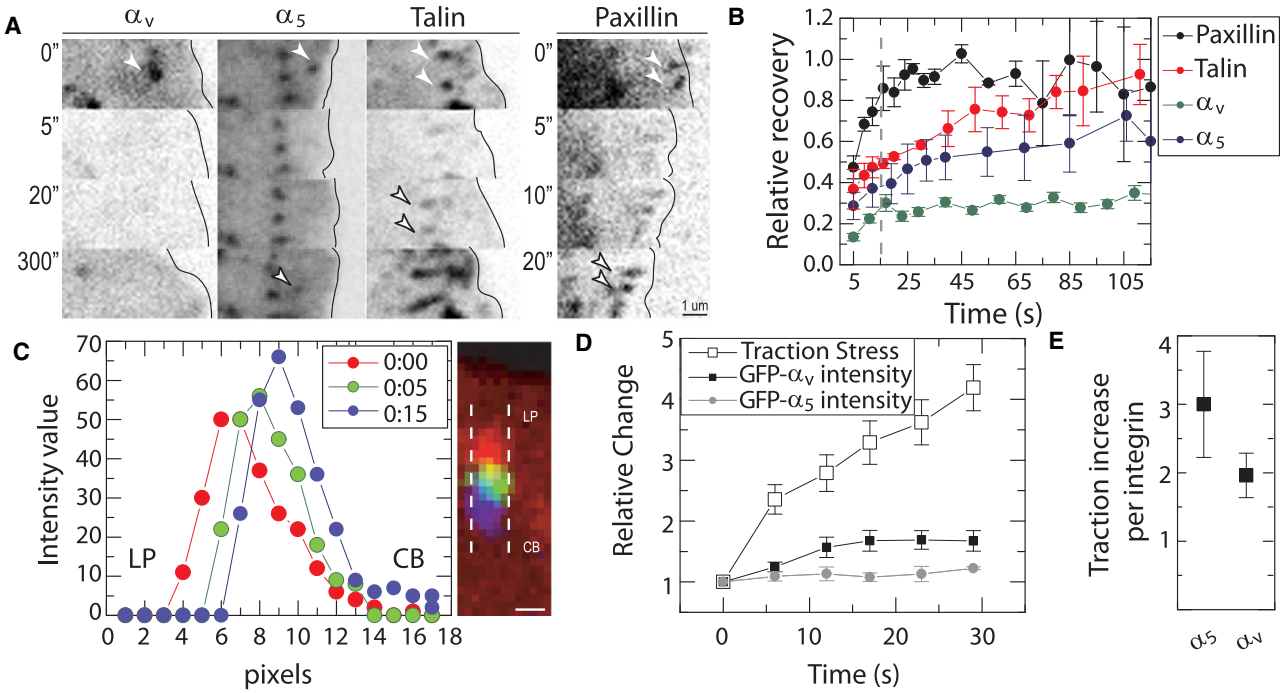

Figure 5. Minimal Exchange of Integrin within FA during Frictional Slip

(A) Vertical montage of images of GFP-tagged α_v, α_5, talin, and paxillin. Prebleached adhesions are shown at t = 0 s (top, white solid arrows), and photobleaching occurred between 0 and 5 s. Post-bleach images are shown for α_v, α_5, talin, and paxillin at the times indicated at left. Times are indicated in seconds. Reappearance of adhesions after bleach in α_5, talin, and paxillin images is indicated by outlined arrows.

(B) Recovery profiles for FA proteins in (A) over time. A dashed line demarcates the termination of the FA slip (t ~ 15 s). Data are shown for 5 FA per protein.

(C) Intensity profiles of GFP-α_v from line scans subtending an individual adhesion at t = 0 s (red), t = 5 s (green), and t = 15 s (blue). Color-combined image of GFP-α_v at times indicated in plot. Dashed lines indicate FA width. The scale bar represents 0.5 μm. LP indicates the lamellipodium, and CB marks the cell body.

(D) Traction stress and integrin fluorescence were normalized to data at t = 0 s and plotted over time. Data reflect average values taken from 18 FAs from five cells.

(E) Ratios of the relative increase in traction stress to the relative change in integrin intensity at the time of adhesion immobilization.

Data plotted in the figure reflect the mean plus standard error about the mean.

changes in fluorescence intensity. To ensure that FRAP measurements of GFP-tagged proteins were performed on adhesions undergoing frictional slip, we confirmed adhesion retrograde movement by visualization with mApple-paxillin and traction-stress increase (data not shown). Both integrins underwent marginal fluorescence recovery (~20%–25%) within the first 20 s after blebbistatin removal (Figures 5A and 5B). At longer times, α_5 underwent partial exchange, whereas α_v underwent negligible turnover.

As a control, we photobleached GFP-talin and GFP-paxillin. For talin, complete recovery was observed over long time scales, on the order of 2 min. In stark contrast, paxillin underwent rapid turnover, which was nearly complete by the end of the slip period (Figures 5A and 5B). Interestingly, the degree of dynamic exchange observed for integrin, talin, and paxillin was similar to that measured in large FAs in U2OS cells under no drug treatment (data not shown) and in other cell types [32]. These results show that integrins remain stably associated to adhesion puncta during frictional slip and do not support polarized remodeling as the predominate mechanism of adhesion translocation.

Force per Available Integrin Increases during Frictional Slip

Our FRAP data indicate stable association of integrin within the adhesion during retrograde slip, suggesting that motion is probably accommodated by a population of integrins that undergo cycles of bond association and dissociation to the ECM while facilitating force transmission [11, 30]. If the apparent adhesion mobility reflects a time scale determined by competing effects of bond association and dissociation, decreased adhesion mobility would be associated with enhanced bond association and diminished bond dissociation for a constant population. Enhanced bond association might result from factors such as changes in integrin activation, a conformational change of integrin required for integrin-ECM binding. However, our data show that enhanced integrin activation via Mn^{2+} treatment [33, 34] did not perturb the dynamics of frictional slip (Figure S6).

Alternatively, if bond dissociation is enhanced under increased force, then increasing the total number of integrins, while maintaining a constant binding kinetics would provide a lower force per integrin and, thus, decrease the rate of integrin unbinding [11]. To probe the changes in the total number of integrins contained within the adhesion during frictional slip, we measured the total GFP-α_v or GFP-α_5 integrin fluorescence intensity within FA. During the slip period (t < 15 s), GFP-α_v intensity increased by approximately 1.5-fold and attained a steady state shortly thereafter (Figures 5C and 5D). By contrast, GFP-α_5 intensity did not undergo appreciable increase during slip or after adhesions engaged the substrate. Because the traction stress increased 3-fold during this time,

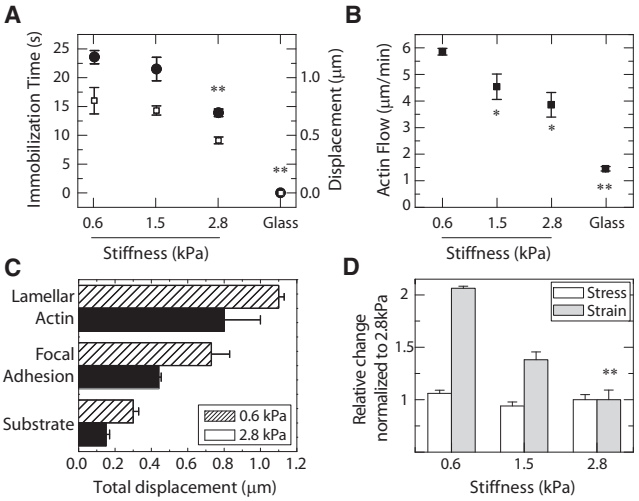

Figure 6. FA Slip Modulated by ECM Stiffness

(A) Adhesion immobilization time (open squares, left) and total displacement during adhesion slip (solid circles, right) plotted against substrate stiffness.
(B) Lamellar F-actin retrograde flow at the onset of blebbistatin removal is plotted against substrate stiffness.
(C) Total displacement during adhesion slip is plotted for F-actin, adhesions, and substrate on 2.8 kPa and 0.6 kPa gels.
(D) Relative (normalized to the 2.8 kPa case) changes in substrate strain (deformation) and traction stress (force) for different substrate stiffnesses. Sample size distribution: glass (n_{FA} = 8, n_{cell} = 2), 2.8 kPa (n_{FA} = 36, n_{cell} = 5), 1.5 kPa (n_{FA} = 8, n_{cell} = 3), and 0.6 kPa (n_{FA} = 8, n_{cell} = 3). P values for data compared to 0.6 kPa case; *$p < 0.01$ and **$p < 0.001$.
Data plotted in the figure reflect the mean plus standard error about the mean.

the average tension per available integrin increased during frictional slip by approximately 2- to 3-fold for both α_v and α_5 integrins (Figure 5E). These data suggest that changes in adhesion strength during frictional slip are not mediated entirely by increases in the total number of integrins available for ligand binding.

Frictional Slip of FAs Is Modulated by the Elastic Stiffness of the ECM

The contrasting mobility of nascent adhesions on soft and rigid substrates during the process of FA maturation suggests that frictional slip may be intimately coupled to ECM stiffness. We sought to determine how changing ECM stiffness modifies the frictional slip of small adhesions near the cell periphery by plating cells on matrices with varied elastic stiffness and glass coverslips. Consistent with previous reports, cells plated on soft (0.6 kPa) gels displayed smaller adhesions and fewer compact F-actin bundles than cells plated on stiffer (2.8 kPa and glass) substrates (Figure S7A).

In the presence of blebbistatin, the differences in cytoskeletal morphology between cells plated on soft and stiff matrices were largely eliminated. Cells plated on soft matrices contained an isotropic network of F-actin throughout the lamella and had a band of small (0.5 μm) adhesions near the LLB (Figure S7B and Movie S6). For matrices with a stiffness less than 2.8 kPa, retrograde frictional slip of adhesion puncta was also observed upon blebbistatin removal (Figure 6A; Figures S7B and S7C; Movie S6 and Movie S7). By contrast, retrograde displacement of adhesions was not resolved on glass (~10^6 kPa) coverslips (Figure 6A; Figure S7D). Perturbing the fibronectin concentration or changing the ECM ligand to collagen did not alter the magnitude or duration of retrograde displacement of adhesions (Figure S6). Thus, ECM stiffness was the predominant regulator of frictional slip. As the ECM stiffness decreased, the total retrograde displacement of the adhesion increased from <200 nm to 0.8 μm, and the time before adhesion immobilization increased from 0 to 25 s (Figure 6A). Interestingly, during frictional slip, the FAs of cells in different mechanical environments are indistinguishable in size; elongation of FA plaques occurs only after engagement to the ECM.

The initial lamellar F-actin flow rate upon release from blebbistatin also depended on the stiffness of the underlying ECM; it increased from 1.5 μm/min on glass to nearly 6 μm/min on 0.6 kPa gels (Figure 6B). Furthermore, the extent of lamellar F-actin retrograde displacement prior to adhesion engagement also varied on matrices of different stiffness; it increased from 0.8 μm on 2.8 kPa gels to 1.1 μm on 0.6 kPa gels (Figure 6C). The displacement of lamellar F-actin always exceeded the retrograde displacement of the nascent adhesion, which in turn was larger than the substrate deformation (Figure 6C). Collectively, these data indicate that the absolute retrograde displacement of the F-actin adhesions and ECM during frictional slip depends on the ECM stiffness.

Frictional Slip of Adhesion Is Abrogated at a Constant Tension

Because the abrogation of adhesion frictional slip occurred concomitantly with increased tension and deformation of the extracellular matrix, we sought to determine whether the immobilization of adhesions to the ECM under myosin II driven tension was a stress (e.g., tension)- or strain (e.g., deformation)-limited process. To explore this, we examined the stress and strain incurred in the substrate at the time of FA engagement for cells plated on matrices with varied elastic stiffness. Modifications to the substrate stiffness change the relationship between the amount of substrate deformation and the magnitude of tension stored within the substrate. As the substrate stiffness decreases, the amount of deformation required to attain a certain amount of tension increases proportionally. We observed that the magnitude of substrate deformation incurred at the time of FA engagement decreased monotonically as its stiffness increased from 0.6 to 2.8 kPa (Figure 6D). By contrast, the traction stress exerted on the substrate at the time of adhesion engagement was similar for all three substrate stiffnesses and amounted to an approximately 30 Pa increase over the traction stress exerted during blebbistatin treatment (Figure 6D). This indicates that the myosin II-driven transition between FA frictional slip and immobilization to ECM occurs at a constant tension, rather than a constant deformation.

Discussion

We have identified a key biophysical transition that occurs as myosin II tension is applied to adhesions. In the absence of myosin II activity, polymerization-dependent nascent adhesions form at the base of the lamellipodium (Figure 7A). When myosin II tension is applied to the lamellar F-actin network, adhesions undergo a transient, rapid, micron-scale rearward translocation while exerting traction against the underlying substrate in a process we term "frictional slip." During frictional slip, traction stress builds and the retrograde F-actin speed slows. Frictional slip is abrogated once a certain

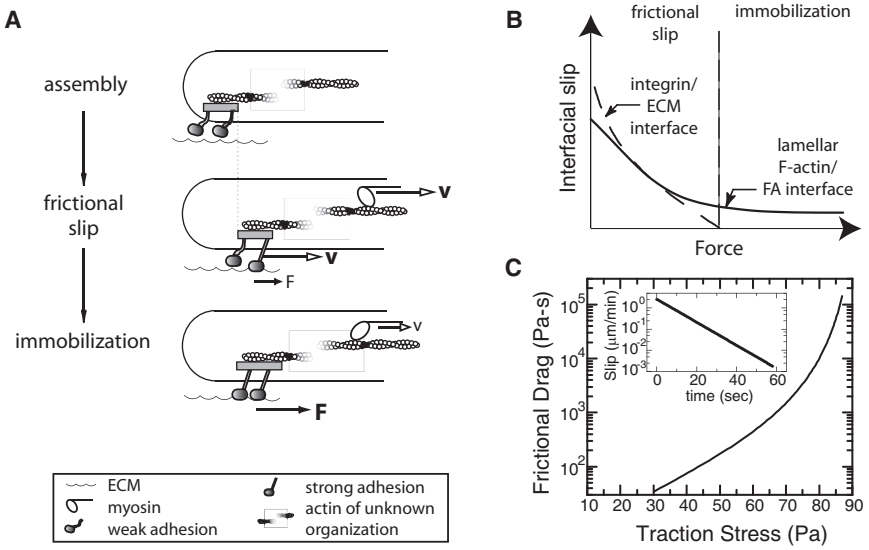

Figure 7. Force-Dependent "Clutch" between Integrin and the ECM

(A) Schematic diagram illustrating mobility of cytoskeletal components at different levels of force. Adhesion assembly: integrins are weakly coupled to the ECM. Frictional slip: myosin II drives fast retrograde velocity of F-actin and associated integrins (*v*, open arrow); traction force magnitude is low (small F, solid arrow). Adhesion immobilization: at a critical tension, integrin-ECM immobilization occurs, traction force increases, myosin-dependent actin flow slows, and FA elongation commences.

(B) Schematic diagram showing that interfacial slip between integrin and the ECM (dashed line) dominates in early adhesions under low force, whereas slip at the actin-FA interface (solid line) dominates and persists in large adhesions under high force.

(C) Semi-log plot of frictional-drag coefficient versus traction stress, determined by calculation based on interpolated data points shown in Figure S7C. Inset: A semi-log plot of the integrin-ECM slip rate versus time after blebbistatin removal was calculated from interpolated data from Figure S7C.

level of force is attained, thereby providing a stable adhesion to further increase force and adhesion elongation.

The rigidity of the ECM regulates the spatiotemporal properties of adhesion frictional slip, such that adhesions displace over longer times and greater distances on softer matrices. With increasing substrate rigidity, the magnitude of rearward translocation decreases such that, for matrices stiffer than ~10 kPa, we estimate that the magnitude of adhesion translocation will not be resolved by light microscopy. This is consistent with observations of FA assembly dynamics on rigid glass coverslips, where nascent FAs seem to be immobilized immediately upon their appearance (Figure 1) [35].

During the transient frictional slip, the integrins move with multiple FA components and colocalized actin. Thus, the retrograde motion of the F-actin is efficiently transmitted to the integrin. After integrins stabilize relative to the ECM, lamellar F-actin retrograde flow persists. This is consistent with previous experiments, which have found movement between actin and FA proteins within mature FAs [15, 16, 36, 37]. This suggests that the initial steps of myosin II-applied tension to FAs are characterized by a transition from a state dominated by slip between integrins and the ECM to one dominated by slip between intracellular FA proteins and F-actin (Figure 7B). We speculate that the location of slip is reflective of the "weakest link" in the actin-FA-ECM connection and that the locations of such "weak links" change during adhesion maturation.

The micron-scale movement of adhesions occurs simultaneously with force exertion onto the ECM. This indicates that bonds between the actin cytoskeleton and ECM exist, but the scale of motion is much larger than could be accommodated by deformation of individual molecular bonds. The strong correlation observed between the motion dynamics of numerous adhesion proteins and the FRAP data demonstrating minimal integrin turnover both suggest a stable association of integrins to the FAs during frictional slip. This leads us to speculate that binding kinetics between integrin and the ECM are regulating frictional slip such that detachment and reattachment at bonds between integrins and the ECM would explain the simultaneous force transduction and retrograde movement. A population of such integrins, constituting an adhesion, could allow some to detach, relieve stress, and reattach while others temporarily transfer the force. Quantitative models incorporating binding kinetics have been successfully used for modeling the differential motion observed between F-actin and FA proteins [11, 30] as well as for modeling other types of adhesive interactions [38].

Increasing amounts of force occurs concomitantly with decreased retrograde movement, indicating that the strength of the integrin-ECM interface increases during frictional slip. This strength can be estimated by the frictional drag coefficient, $\sigma_{TR}/[A(v_{FA} - v_S)]$, where σ_{TR} is the traction stress exerted to the underlying matrix, $v_{FA} - v_S$ is the difference in flow speed between FA and the substrate (Figure 7C, inset), and A is the approximate area of nascent adhesions ($A \sim 0.1\ \mu m^2$). A calculation of the frictional-drag coefficient from interpolation of our experimental data yields a frictional-drag coefficient of the integrin-ECM interface that rapidly rises nearly 100-fold as the applied traction increases from 30 to 70 Pa (Figure 7C). Because little to no accumulation of new integrin is observed within adhesions during this time, we hypothesize that this aggregate bond strengthening occurs predominately through bond reorganization via integrin clustering [39, 40] or through force-induced changes in individual bond strength between the integrin and ECM [41, 42]. Future experiments will be needed to dissect the underlying mechanisms of this strengthening as well as to explore the impact of different integrin-ECM interactions.

In summary, we have found that bonds between the integrin and extracellular matrix function as an extracellular "clutch" to modulate the degree of force transmission from the F-actin cytoskeleton to the extracellular matrix in early-stage myosin II-mediated FA maturation. The rapid strengthening of the integrin-ECM interface at small loads would enable protrusions at the leading cell edge to be weakly adherent and mechanically sense the external matrix without rigid attachment. During this initial stage of substrate sensing, the retrograde flow dynamics of the actomyosin cytoskeleton play a prominent role in rapidly building tension to stabilize integrin binding to ECMs with varied mechanical compliance. However, under sufficient tension generated by actomyosin contraction, this

adhesion would stabilize to impede the retrograde motion of the F-actin and immobilize FA plaques to mediate further FA elongation and growth. This underscores the importance of mechanical feedback between the F-actin cytoskeleton and the ECM in building force-sensitive adhesions that control cell motility and morphology.

Experimental Procedures

Cell Culture and Transfection

Human osteosarcoma (U2OS) cells were obtained from American Type Culture Collection (ATCC) and maintained in McCoy's medium (HyClone), supplemented with 10% fetal bovine serum (HyClone), penicillin, and streptomycin (GIBCO). Transient transfections of GFP-actin (C. Waterman, NIH), mApple-paxillin, GFP-vinculin (M. Davidson, U. of Florida), GFP-α_5 integrin (R. Horwitz, U. of Virginia), GFP-α_v integrin, and GFP-talin (K. Hu, U. of Indiana) were performed with FuGENE6 Transfection Reagent (Roche) per the manufacturer's instructions.

Immunofluorescence

Immunofluorescence of myosin light chain (monoclonal, Cell Signaling), paxillin (polyclonal, Santa Cruz), vinculin (monoclonal, Sigma), fibronectin (polyclonal, Sigma), and phalloidin (Molecular Probes) staining of F-actin was performed as previously described [18].

Preparation of Polyacrylamide (PAA) Substrates for Traction Force Microscopy

Fibronectin-coated PAA substrates containing 40 nm fluorescent spheres were prepared on glass coverslips [10, 43] with varying acrylamide/bisacrylamide ratios so that gels with varying elastic moduli could be obtained: 7.5%/0.1% for 2.8 kPa, 7.5%/0.05% for 1.5kPa, and 5%/0.075% for 0.6 kPa, as characterized previously [3]. Fibronectin or collagen was covalently attached to the top surface of the PAA gel via the bifunctional cross-linker sulfo-SANPAH (Pierce).

Live Cell Microscopy

Coverslips containing transfected cells bound to PAA substrates were mounted in a perfusion chamber (Warner Instruments) in imaging media consisting of media supplemented with 30 μl/1 ml Oxyrase (Oxyrase Enzyme system, EC0050) and 10 mM HEPES (pH 7.5). Cells were imaged at 37°C 24–48 hr after transfection on a multispectral spinning-disk confocal microscope consisting of a Nikon Ti with a 60× 1.2 NA plan Apo WI objective lens (Nikon) and a CSUX scanner (Yokogawa). A CCD camera (Coolsnap HQ2, Photometrics) controlled with Metamorph acquisition software (MDS Analytical Technologies) was used. FAs and beads were monitored at the same confocal section; F-actin was imaged 0.2 μm into the cell interior.

Cells were treated with 25–50 μM blebbistatin (Sigma) for 30 min [25]. For blebbistatin inactivation, cells were washed with imaging media and visualized with 488 nm light [21].

Image Analysis

Particle Imaging Velocimetry code in MATLAB (mpiv, developed by N. Mori and K-A Chang) was used for identifying, with sub-pixel accuracy, the movement of beads embedded in polyacrylamide substrate. Fourier transform traction cytometry methods were used for determining traction stress from bead displacements [43]. Traction stresses documented in the text were calculated as an average of the maximum values across individual FAs.

Fiducial marks of fluorescent F-actin, centroids of FAs, and substrate-embedded beads were tracked in separate image channels with computational tracking software developed by the lab of Gaudenz Danuser [24]. Manual tracking, via the point tracking function in Metamorph, of F-actin patches associated with FA puncta was used as an alternative method.

Velocity vector fields were interpolated onto linescans subtending individual FA puncta (perpendicular to the cell edge) via a Gaussian-weighted interpolation, with a full-width half maximum of 10 pixels (1 μm). All vector fields exhibited a high degree of directional coupling [10]. Lamellar F-actin flow vectors were measured 1.2 μm proximal to the FA centroids (Figure S3A).

FA engagement time was defined as the time at which the displacement rate of FA puncta converged with that of beads within the PAA gel (error of 0.02 μm/min).

Length changes in FAs and actin bundles were quantified in Metamorph. Fluorescence intensity of GFP-α_5 and GFP-α_v was background subtracted, integrated across the FA area, and normalized to the first image plane.

Data plotted in figures reflect the mean plus standard error about the mean.

FRAP

Photobleaching experiments were performed with a 405 nm laser coupled through a micromirror array to control the spatial location of illumination (Mosaic, Photonics Instruments) with a 200 ms exposure time and a rectangular region of approximately 5 μm^2. The photobleaching event took place after acquisition of the first image after blebbistatin removal, and post-bleach images were recorded thereafter. Analysis was performed as in [44].

Supplemental Information

Supplemental Information includes seven figures and seven movies and can be found with this article online at doi:10.1016/j.cub.2010.05.049.

Acknowledgments

The authors wish to acknowledge use of computational-analysis algorithms for analyzing cytoskeletal dynamics and traction forces developed in the labs of Gaudenz Danuser and Ulrich Schwarz, respectively, as well as generous gifts of cDNA constructs used in this paper: GFP-actin (C. Waterman, NIH), mApple-paxillin (M. Davidson, U. of Florida), GFP-α_5 integrin (R. Horwitz, U. of Virginia), and GFP-α_v integrin and GFP-talin (Ke Hu, U. of Indiana). Experiments visualizing fibronectin mobility during adhesion slip were conducted by S.P. Winter. The authors would like to thank Y. Beckham, P. Oakes, and T. Schaus for helpful comments and careful reading of the manuscript. This work was supported by a Burroughs Wellcome Career Award, a Keck Foundation Grant, and an NIH Director's Pioneer Award (DP10D00354) to M.L. Gardel.

Received: March 9, 2010
Revised: April 20, 2010
Accepted: May 14, 2010
Published online: June 10, 2010

References

1. Berrier, A.L., and Yamada, K.M. (2007). Cell-matrix adhesion. J. Cell. Physiol. *213*, 565–573.
2. Vicente-Manzanares, M., Choi, C.K., and Horwitz, A.R. (2009). Integrins in cell migration—The actin connection. J. Cell Sci. *122*, 199–206.
3. Yeung, T., Georges, P.C., Flanagan, L.A., Marg, B., Ortiz, M., Funaki, M., Zahir, N., Ming, W., Weaver, V., and Janmey, P.A. (2005). Effects of substrate stiffness on cell morphology, cytoskeletal structure, and adhesion. Cell Motil. Cytoskeleton *60*, 24–34.
4. Schwartz, M.A., and DeSimone, D.W. (2008). Cell adhesion receptors in mechanotransduction. Curr. Opin. Cell Biol. *20*, 551–556.
5. Choquet, D., Felsenfeld, D.P., and Sheetz, M.P. (1997). Extracellular matrix rigidity causes strengthening of integrin-cytoskeleton linkages. Cell *88*, 39–48.
6. Chrzanowska-Wodnicka, M., and Burridge, K. (1996). Rho-stimulated contractility drives the formation of stress fibers and focal adhesions. J. Cell Biol. *133*, 1403–1415.
7. Balaban, N.Q., Schwarz, U.S., Riveline, D., Goichberg, P., Tzur, G., Sabanay, I., Mahalu, D., Safran, S., Bershadsky, A., Addadi, L., and Geiger, B. (2001). Force and focal adhesion assembly: A close relationship studied using elastic micropatterned substrates. Nat. Cell Biol. *3*, 466–472.
8. Alexandrova, A.Y., Arnold, K., Schaub, S., Vasiliev, J.M., Meister, J.J., Bershadsky, A.D., and Verkhovsky, A.B. (2008). Comparative dynamics of retrograde actin flow and focal adhesions: Formation of nascent adhesions triggers transition from fast to slow flow. PLoS ONE *3*, e3234.
9. Zhang, X., Jiang, G., Cai, Y., Monkley, S.J., Critchley, D.R., and Sheetz, M.P. (2008). Talin depletion reveals independence of initial cell spreading from integrin activation and traction. Nat. Cell Biol. *10*, 1062–1068.
10. Gardel, M.L., Sabass, B., Ji, L., Danuser, G., Schwarz, U.S., and Waterman, C.M. (2008). Traction stress in focal adhesions correlates biphasically with actin retrograde flow speed. J. Cell Biol. *183*, 999–1005.

11. Chan, C.E., and Odde, D.J. (2008). Traction dynamics of filopodia on compliant substrates. Science *322*, 1687–1691.
12. Jurado, C., Haserick, J.R., and Lee, J. (2005). Slipping or gripping? Fluorescent speckle microscopy in fish keratocytes reveals two different mechanisms for generating a retrograde flow of actin. Mol. Biol. Cell *16*, 507–518.
13. Mitchison, T., and Kirschner, M. (1988). Cytoskeletal dynamics and nerve growth. Neuron *1*, 761–772.
14. Jiang, G., Giannone, G., Critchley, D.R., Fukumoto, E., and Sheetz, M.P. (2003). Two-piconewton slip bond between fibronectin and the cytoskeleton depends on talin. Nature *424*, 334–337.
15. Brown, C.M., Hebert, B., Kolin, D.L., Zareno, J., Whitmore, L., Horwitz, A.R., and Wiseman, P.W. (2006). Probing the integrin-actin linkage using high-resolution protein velocity mapping. J. Cell Sci. *119*, 5204–5214.
16. Hu, K., Ji, L., Applegate, K.T., Danuser, G., and Waterman-Storer, C.M. (2007). Differential transmission of actin motion within focal adhesions. Science *315*, 111–115.
17. Webb, D.J., Donais, K., Whitmore, L.A., Thomas, S.M., Turner, C.E., Parsons, J.T., and Horwitz, A.F. (2004). FAK-Src signalling through paxillin, ERK and MLCK regulates adhesion disassembly. Nat. Cell Biol. *6*, 154–161.
18. Gupton, S.L., and Waterman-Storer, C.M. (2006). Spatiotemporal feedback between actomyosin and focal-adhesion systems optimizes rapid cell migration. Cell *125*, 1361–1374.
19. Straight, A.F., Cheung, A., Limouze, J., Chen, I., Westwood, N.J., Sellers, J.R., and Mitchison, T.J. (2003). Dissecting temporal and spatial control of cytokinesis with a myosin II Inhibitor. Science *299*, 1743–1747.
20. Verkhovsky, A.B., Svitkina, T.M., and Borisy, G.G. (1995). Myosin II filament assemblies in the active lamella of fibroblasts: Their morphogenesis and role in the formation of actin filament bundles. J. Cell Biol. *131*, 989–1002.
21. Sakamoto, T., Limouze, J., Combs, C.A., Straight, A.F., and Sellers, J.R. (2005). Blebbistatin, a myosin II inhibitor, is photoinactivated by blue light. Biochemistry *44*, 584–588.
22. Riveline, D., Zamir, E., Balaban, N.Q., Schwarz, U.S., Ishizaki, T., Narumiya, S., Kam, Z., Geiger, B., and Bershadsky, A.D. (2001). Focal contacts as mechanosensors: Externally applied local mechanical force induces growth of focal contacts by an mDia1-dependent and ROCK-independent mechanism. J. Cell Biol. *153*, 1175–1186.
23. Danuser, G., and Waterman-Storer, C.M. (2006). Quantitative fluorescent speckle microscopy of cytoskeleton dynamics. Annu. Rev. Biophys. Biomol. Struct. *35*, 361–387.
24. Ji, L., and Danuser, G. (2005). Tracking quasi-stationary flow of weak fluorescent signals by adaptive multi-frame correlation. J. Microsc. *220*, 150–167.
25. Hotulainen, P., and Lappalainen, P. (2006). Stress fibers are generated by two distinct actin assembly mechanisms in motile cells. J. Cell Biol. *173*, 383–394.
26. Geiger, B., Spatz, J.P., and Bershadsky, A.D. (2009). Environmental sensing through focal adhesions. Nat. Rev. Mol. Cell Biol. *10*, 21–33.
27. Le Clainche, C., and Carlier, M.-F. (2008). Regulation of actin assembly associated with protrusion and adhesion in cell migration. Physiol. Rev. *88*, 489–513.
28. Galbraith, C.G., Yamada, K.M., and Sheetz, M.P. (2002). The relationship between force and focal complex development. J. Cell Biol. *159*, 695–705.
29. Ballestrem, C., Hinz, B., Imhof, B.A., and Wehrle-Haller, B. (2001). Marching at the front and dragging behind: Differential alphaVbeta3-integrin turnover regulates focal adhesion behavior. J. Cell Biol. *155*, 1319–1332.
30. Macdonald, A., Horwitz, A.R., and Lauffenburger, D.A. (2008). Kinetic model for lamellipodal actin-integrin 'clutch' dynamics. Cell Adh Migr *2*, 95–105.
31. Wehrle-Haller, B., and Imhof, B. (2002). The inner lives of focal adhesions. Trends Cell Biol. *12*, 382–389.
32. Lele, T.P., Thodeti, C.K., Pendse, J., and Ingber, D.E. (2008). Investigating complexity of protein-protein interactions in focal adhesions. Biochem. Biophys. Res. Commun. *369*, 929–934.
33. Mould, A.P., Askari, J.A., Barton, S., Kline, A.D., McEwan, P.A., Craig, S.E., and Humphries, M.J. (2002). Integrin activation involves a conformational change in the alpha 1 helix of the beta subunit A-domain. J. Biol. Chem. *277*, 19800–19805.
34. Chen, J., Salas, A., and Springer, T.A. (2003). Bistable regulation of integrin adhesiveness by a bipolar metal ion cluster. Nat. Struct. Biol. *10*, 995–1001.
35. Choi, C.K., Vicente-Manzanares, M., Zareno, J., Whitmore, L.A., Mogilner, A., and Horwitz, A.R. (2008). Actin and alpha-actinin orchestrate the assembly and maturation of nascent adhesions in a myosin II motor-independent manner. Nat. Cell Biol. *10*, 1039–1050.
36. Guo, W.H., and Wang, Y.L. (2007). Retrograde fluxes of focal adhesion proteins in response to cell migration and mechanical signals. Mol. Biol. Cell *18*, 4519–4527.
37. Wang, Y.L. (2007). Flux at focal adhesions: Slippage clutch, mechanical gauge, or signal depot. Sci. STKE *2007*, pe10.
38. Thomas, W. (2008). Catch bonds in adhesion. Annu. Rev. Biomed. Eng. *10*, 39–57.
39. Selhuber-Unkel, C., López-García, M., Kessler, H., and Spatz, J.P. (2008). Cooperativity in adhesion cluster formation during initial cell adhesion. Biophys. J. *95*, 5424–5431.
40. Roca-Cusachs, P., Gauthier, N.C., del Rio, A., and Sheetz, M.P. (2009). Clustering of alpha(5)beta(1) integrins determines adhesion strength whereas alpha(v)beta(3) and talin enable mechanotransduction. Proc. Natl. Acad. Sci. USA *106*, 16245–16250.
41. Kong, F., García, A.J., Mould, A.P., Humphries, M.J., and Zhu, C. (2009). Demonstration of catch bonds between an integrin and its ligand. J. Cell Biol. *185*, 1275–1284.
42. Friedland, J.C., Lee, M.H., and Boettiger, D. (2009). Mechanically activated integrin switch controls alpha5beta1 function. Science *323*, 642–644.
43. Sabass, B., Gardel, M.L., Waterman, C.M., and Schwarz, U.S. (2008). High resolution traction force microscopy based on experimental and computational advances. Biophys. J. *94*, 207–220.
44. Aratyn, Y.S., Schaus, T.E., Taylor, E.W., and Borisy, G.G. (2007). Intrinsic dynamic behavior of fascin in filopodia. Mol. Biol. Cell *18*, 3928–3940.